Available online at www.sciencedirect.com
ScienceDirect
Corrosion Science 48 (2006) 4020–4036
CORROSION SCIENCE
www.elsevier.com/locate/corsci

The third-element effect in the oxidation of Ni–xCr–7Al ($x = 0$, 5, 10, 15 at.%) alloys in 1 atm O_2 at 900–1000 °C

Y. Niu [a,*], X.J. Zhang [a,b], Y. Wu [a], F. Gesmundo [c]

[a] *State Key Laboratory for Corrosion and Protection, Institute of Metal Research, Chinese Academy of Science, Wencui Road 62, 110016 Shenyang, China*
[b] *Shenyang Institute of Chemical Technology, 110142 Shenyang, China*
[c] *DICheP – Università di Genova, Fiera del Mare, Pad.D, 16129 Genova, Italy*

Received 16 May 2005; accepted 16 March 2006
Available online 24 May 2006

Abstract

The oxidation in 1 atm of pure oxygen of Ni–Cr–Al alloys with a constant aluminum content of 7 at.% and containing 5, 10 and 15 at.% Cr was studied at 900 and 1000 °C and compared to the behavior of the corresponding binary Ni–Al alloy (Ni–7Al). A dense external scale of NiO overlying a zone of internal oxide precipitates formed on Ni–7Al and Ni–5Cr–7Al at both temperatures. Conversely, an external Al_2O_3 layer formed on Ni–10Cr–7Al at both temperatures and on Ni–15Cr–7Al at 900 °C, while the scales grown initially on Ni–15Cr–7Al at 1000 °C were more complex, but eventually developed an innermost protective alumina layer. Thus, the addition of sufficient chromium levels to Ni–7Al produced a classical third-element effect, inducing the transition between internal and external oxidation of aluminum. This effect is interpreted on the basis of an extension to ternary alloys of a criterion first proposed by Wagner for the transition between internal and external oxidation of the most reactive component in binary alloys.

Keywords: Ternary alloys; Ni–Cr–Al; Oxidation; Third-element effect

* Corresponding author. Tel.: +86 24 8389 0021; fax: +86 24 2389 3624.
E-mail address: yniu@imr.ac.cn (Y. Niu).

0010-938X/$ - see front matter © 2006 Elsevier Ltd. All rights reserved.
doi:10.1016/j.corsci.2006.03.008

1. Introduction

For applications in oxygen-rich environments at very high temperatures, alloys and coatings are often designed to develop surface layers of Al_2O_3, which, unlike Cr_2O_3, does not form higher volatile oxides [1–3]. The development of Al_2O_3 scales on Ni-, Fe- and Co-based binary alloys is possible using sufficiently high aluminum contents (6–12 wt.%) [1–7]. Unfortunately, these aluminum levels in binary alloys often result in unacceptable mechanical properties. The Ni–Cr–Al system forms a γ–γ' structure that exhibits improved mechanical properties and better oxidation resistance than the corresponding binary alloys [8]. Therefore, this system became a basis for the development of more oxidation-resistant materials by the addition of further alloying elements. In practice, adding chromium to Ni–Al alloys decreases the concentration of aluminum required to establish the Al_2O_3 scale [1,9]. This is an example of a more general phenomenon of considerable practical importance, called the third-element effect (TEE), by which the presence of a third element with a reactivity intermediate to the components of the given binary alloy can decrease the content of the more reactive element needed to form its external oxide scale on ternary alloys compared to binary alloys.

According to an initial suggestion by Wagner [10], the third element, e.g. chromium in M–Al alloys, acts as a getter for oxygen in the alloy during the initial stage, lowering the oxygen solubility in the alloy and preventing internal oxidation of the more reactive component, aluminum, producing external Al_2O_3 layers at lower aluminum levels than in binary M–Al alloys. Various mechanisms have been proposed so far to explain TEE, as summarized by Stott et al. [1], considering possible ways to avoid the internal oxidation. One of the possible explanations, originally advanced by Giggins and Pettit [9], attributes this effect to the simultaneous precipitation of internal oxides of the two most reactive components in ternary alloys. This process produces an overall volume fraction of internal oxides that reaches the critical value required for the transition to external oxidation, according to a criterion defined by Wagner [11], and thus can prevent the internal oxidation even without involving a reduction of the oxygen solubility predicted by Wagner's model, with contents of the most reactive component that are smaller for ternary than for binary alloys. A semi-quantitative treatment based on this assumption, developed recently [12], is applied here to the oxidation at 900–1000 °C of the present Ni–Cr–Al alloys.

2. Experimental

Three Ni–*x*Cr–7Al alloys containing approximately 7 at.% Al and 5, 10 and 15 at.% Cr (Ni–5Cr–7Al, Ni–10Cr–7Al and Ni–15Cr–7Al) and one Ni–Al alloy with a similar aluminum content (Ni–7Al), were prepared from high-purity metals by arc-melting under a Ti-gettered argon atmosphere using non-consumable tungsten electrodes from appropriate amounts of pure nickel (99.99%), aluminum (99.999%) and chromium (99.99%). The alloy ingots were subsequently annealed in 1 atm argon at 1100 °C for 24 h to remove the residual mechanical stresses and achieve a better alloy equilibration. The actual average compositions of the four alloys (at.%) are 6.6Al, 5.0Cr–6.8Al, 10.0Cr–7.3Al, and 15.0Cr–7.2Al, balance Ni, respectively. The compositions of the same alloys in wt.% are 3.1Al, 4.6Cr–3.3Al, 9.4Cr–3.5Al and 14.1Cr–3.5Al, respectively.

Flat specimens with a surface area of about 2 cm^2 were cut from the ingots by a diamond wheel saw, ground down to 1200 emery paper, washed in water, alcohol and acetone and then dried immediately before use. Oxidation tests were carried out in 1 atm of pure oxygen at 900 and 1000 °C for 24 h with continuous weight-gain measurements using a Cahn thermobalance. The microstructures of the alloys and the oxide scales were characterized by scanning electron microscopy (SEM) with an energy-dispersive X-ray spectrometer (EDS) attached to the SEM to establish the morphology, compositions, and spatial distributions of the compounds formed by oxidation.

3. Results

3.1. Oxidation kinetics

The oxidation kinetics for the four Ni–*x*Cr–7Al alloys at 900 and 1000 °C in 1 atm O_2 are shown in Figs. 1, 2 as linear plots (Figs. 1(a) and 2(a)) and parabolic plots (Figs. 1(b) and 2(b)), respectively. At 900 °C (Fig. 1), the kinetics for Ni–7Al, Ni–5Cr–7Al and Ni–15Cr–7Al obeyed the parabolic rate law to a good approximation for the whole duration

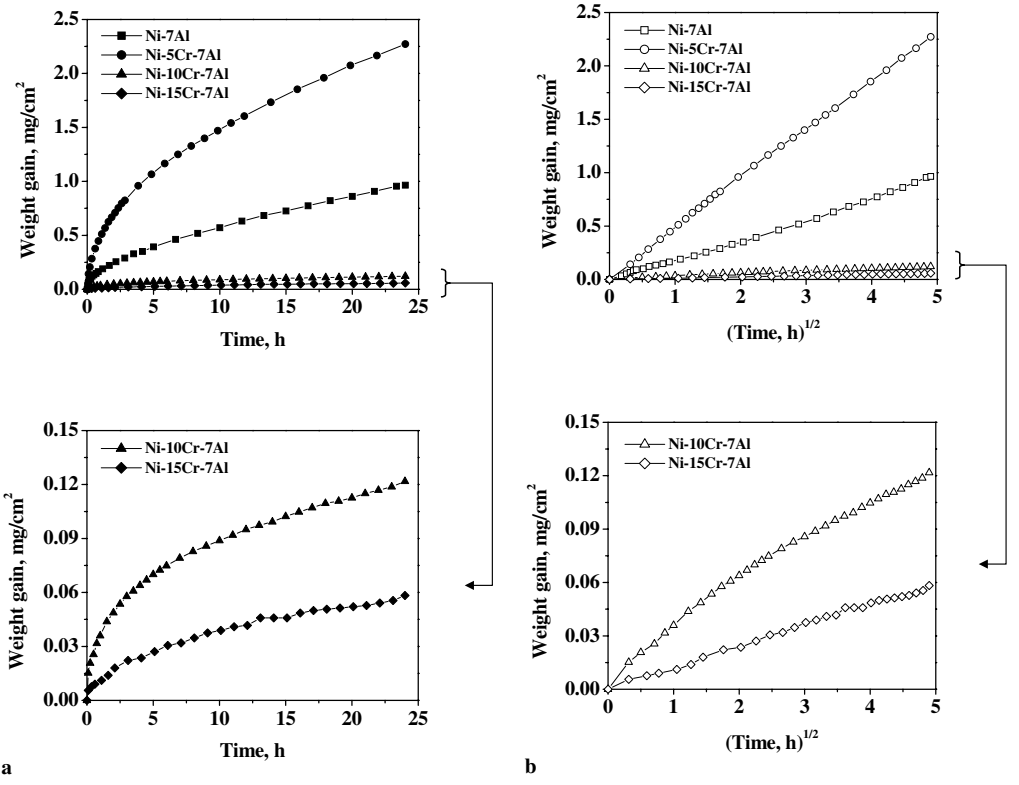

Fig. 1. Kinetics for the four Ni–*x*Cr–7Al ($x = 0, 5, 10, 15$ at.%) alloys oxidized for 24 h at 900 °C in 1 atm of pure O_2: (a) normal plots and (b) parabolic plots.

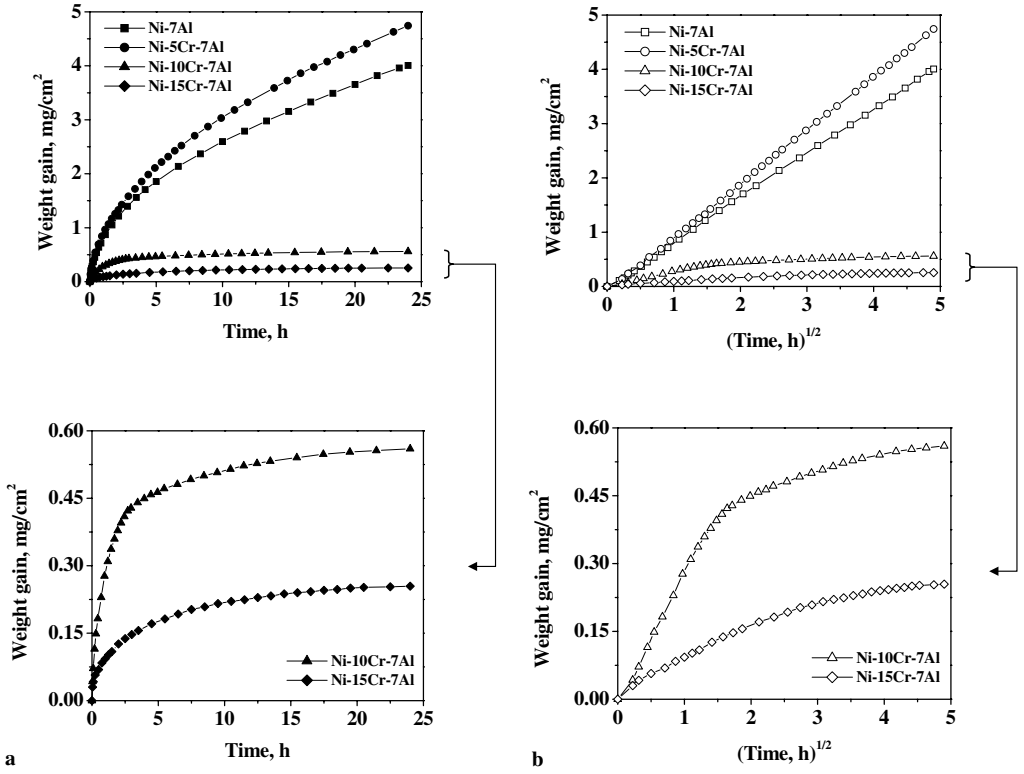

Fig. 2. Kinetics for the four Ni–xCr–7Al ($x = 0$, 5, 10, 15 at.%) alloys oxidized for 24 h at 1000 °C in 1 atm of pure O_2: (a) normal plots and (b) parabolic plots.

of the test. However, the kinetics curve for Ni–10Cr–7Al at 900 °C exhibited a transition from an initial faster nearly parabolic stage, with a rate constant of 2.1×10^{-13} $g^2\ cm^{-4}\ s^{-1}$, lasting about 3 h, to a second parabolic stage with a lower rate constant of about 9.9×10^{-14} $g^2\ cm^{-4}\ s^{-1}$ from 4 to 24 h. At 1000 °C, the kinetics for Ni–7Al and Ni–5Cr–7Al again obeyed approximately the parabolic rate law, while those for Ni–10Cr–7Al and Ni–15Cr–7Al were composed of an initial parabolic stage, with rate constants of 2.4×10^{-11} $g^2\ cm^{-4}\ s^{-1}$ for Ni–10Cr–7Al for the first 1.4 h and 1.4×10^{-12} $g^2\ cm^{-4}\ s^{-1}$ for Ni–15Cr–7Al for the first 2.2 h, respectively. After the first stage, the slopes of the parabolic plots decreased continuously with time to a final value of about 7.7×10^{-14} $g^2\ cm^{-4}\ s^{-1}$ for Ni–10Cr–7Al and 9.9×10^{-14} $g^2\ cm^{-4}\ s^{-1}$ for Ni–15Cr–7Al, respectively (Table 1).

Table 1
Approximate values for the parabolic rate constants ($g^2\ cm^{-4}\ s^{-1)}$ for the four Ni–xCr–7Al alloys ($x = 0$, 5, 10, 15 at.%) at 900 and 1000 °C in 1 atm of pure O_2

	Ni–7Al	Ni–5Cr–7Al	Ni–10Cr–7Al		Ni–15Cr–7Al	
900 °C	1.0×10^{-11}	5.9×10^{-11}	2.1×10^{-13} (in.)	9.9×10^{-14} (fi.)	3.8×10^{-14}	
1000 °C	1.9×10^{-10}	2.7×10^{-10}	2.4×10^{-11} (in.)	7.7×10^{-14} (fi.)	1.4×10^{-12} (in.)	9.9×10^{-14} (fi.)

(in.) = values during the initial stage; (fi.) = values during the final stage.

Altogether, Ni–5Cr–7Al oxidized more rapidly, while the other two alloys corroded more slowly than the corresponding binary Ni–7Al alloy. In particular, the final parabolic rate constants for Ni–10Cr–7Al and Ni–15Cr–7Al were about two to three orders of magnitude smaller than those for Ni–7Al (Table 1).

3.2. Scale morphology and microstructure

The microstructures of the scales formed on Ni–7Al after 24 h at 900 °C and 1000 °C are shown in Fig. 3. At both temperatures, Ni–7Al formed a dense external layer of NiO containing some Ni–Al spinel oxide particles in an inner region corresponding to the alloy consumption zone, followed by a zone of internal oxides of aluminum.

The scale formed on Ni–5Cr–7Al after 24 h oxidation at 900 °C (Fig. 4(a)) was composed of an outer layer of NiO containing an average of about 1 at.% Cr and 2 at.% Al, followed by a region of internal oxides of both aluminum and chromium.

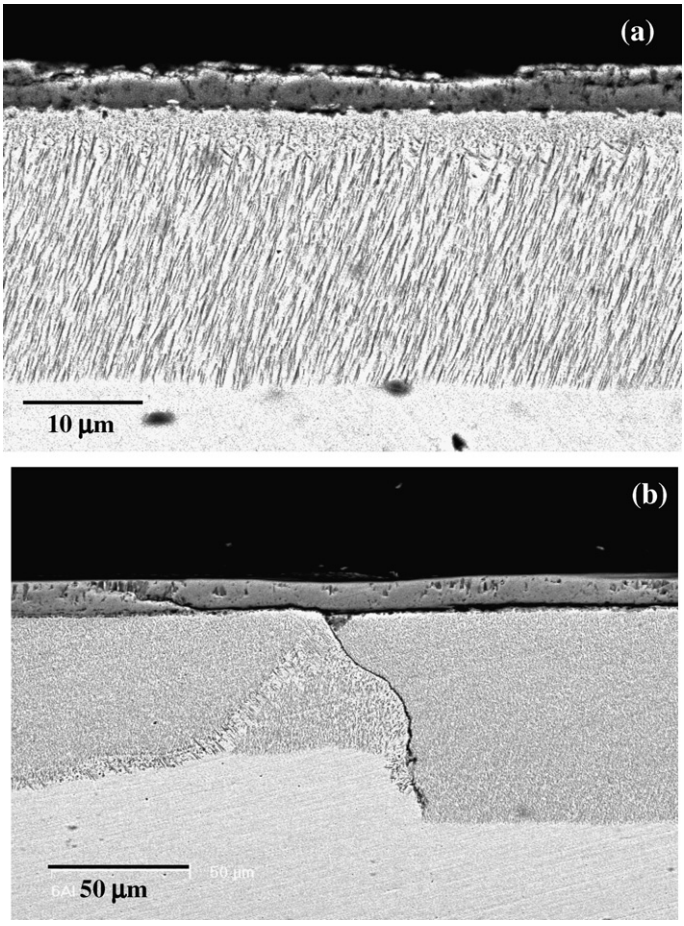

Fig. 3. Micrographs (SEM/BEI) of cross sections of Ni–7Al oxidized for 24 h in 1 atm O_2 at 900 °C (a) and 1000 °C (b).

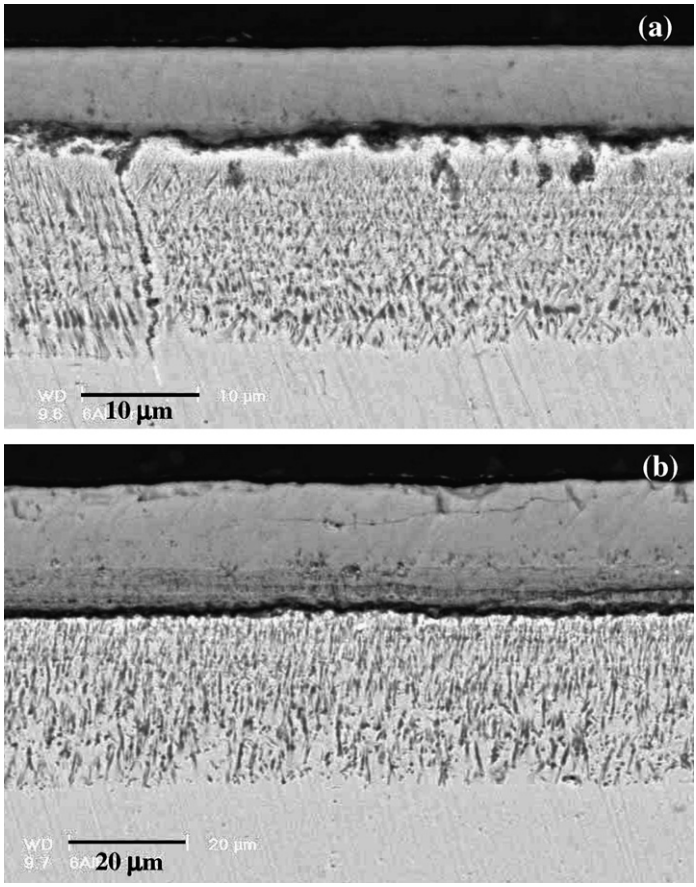

Fig. 4. Micrographs (SEM/BEI) of cross sections of Ni–5Cr–7Al oxidized for 24 h in 1 atm O_2 at 900 (a) and 1000 °C (b).

The chromium and aluminum contents in the scale close to the interface with the alloy were higher than the average values measured in the NiO layer and in the internal oxide zone, suggesting the possible presence of a very thin layer of $Ni(Cr, Al)_2O_4$. After 24 h oxidation at 1000 °C, the scale formed on the same alloy (Fig. 4(b)) contained an outermost NiO layer plus an inner zone of internal oxides of aluminum and chromium. In turn, the NiO layer was composed of two different regions that differed in their chromium and aluminum contents; these were smaller in the outer lighter region than in the inner darker region.

An exclusive and continuous external layer of Al_2O_3 containing about 10 at.% Cr in solution was formed by oxidation of Ni–10Cr–7Al at 900 °C (Fig. 5(a)). Furthermore, the alloy close to the scale was depleted in aluminum (light layer in Fig. 5(a)), while some small voids were present at the alloy/scale interface. Conversely, the scales formed on the same alloy at 1000 °C (Fig. 5(b)) contained an outermost irregular layer of NiO (light) and an innermost continuous layer of Al_2O_3 (dark), plus a continuous intermediate layer (gray)

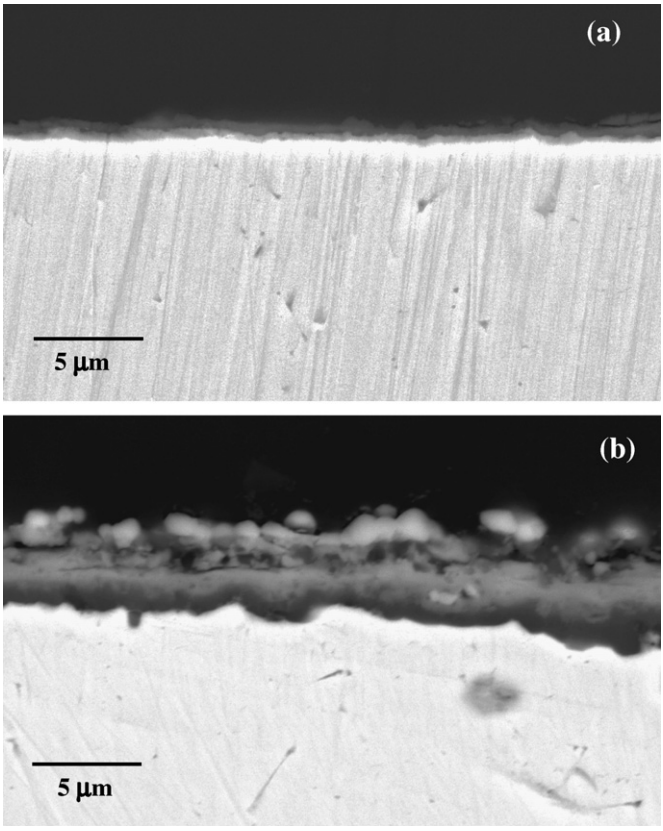

Fig. 5. Micrographs (SEM/BEI) of cross sections of Ni–10Cr–7Al oxidized for 24 h in 1 atm O_2 at 900 (a) and 1000 °C (b).

composed of a mixture of Ni–Al and Ni–Cr spinel oxides. No internal oxidation was observed for this alloy at either temperature.

A very thin regular layer of Al_2O_3 containing less chromium than in the case of Ni–10Cr–7Al (about 5 at.%) formed on Ni–15Cr–7Al by oxidation at 900 °C, as shown in Fig. 6(a). Conversely, the scales formed on this alloy after oxidation at 1000 °C (Fig. 6(b)) were very irregular in thickness and contained two main zones. The outermost medium-gray layer was composed of a mixture of Cr_2O_3 and Ni–Cr spinel oxide, but also contained a significant volume fraction of nickel metal (light areas) that sometimes even formed a discontinuous layer. Beneath this external layer was a region composed of a mixture of alloy and coarse particles of Al_2O_3 (dark), which appeared partly isolated from each other but were also partly interconnected. At locations where the scale was free from metal particles, the external Cr-rich layer had a smaller thickness, while Al_2O_3 was able to form as a continuous layer. The oxidation behavior of Ni–15Cr–7Al at this temperature seems to be intermediate between internal oxidation of aluminum beneath an external Cr_2O_3 scale and the formation of a continuous innermost Al_2O_3 layer. In any case, the internal oxidation of aluminum is unusual due to the large size and the irregular spatial

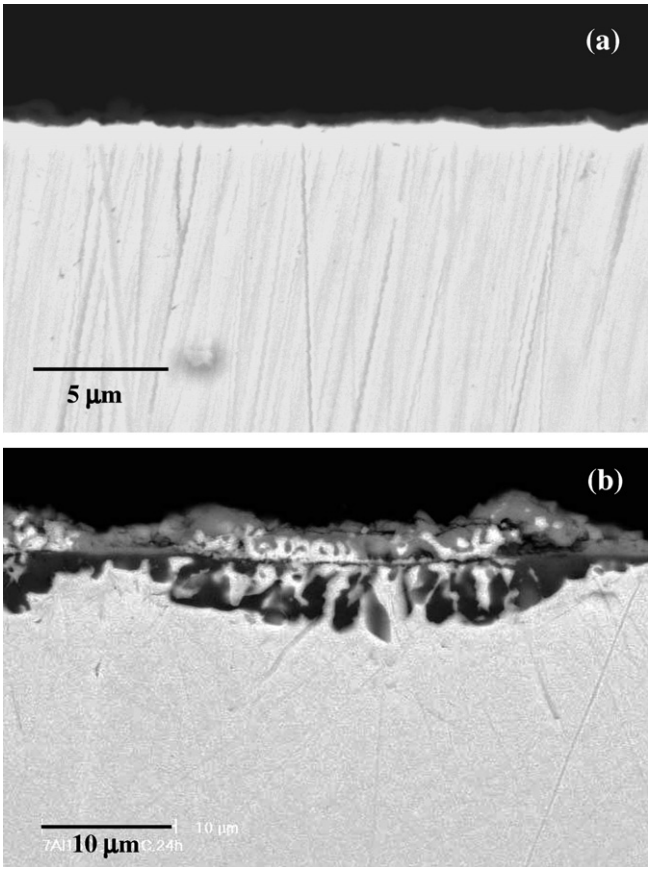

Fig. 6. Micrographs (SEM/BEI) of cross sections of Ni–15Cr–7Al oxidized for 24 h in 1 atm O_2 at 900 (a) and 1000 °C (b).

distribution of the Al_2O_3 particles compared to the normal appearance of the zones of internal oxide on the more dilute alloys.

4. Discussion

4.1. Previous studies of the oxidation of Ni–Al, Ni–Cr and Ni–Cr–Al alloys

Among various studies of the oxidation of binary Ni–Al alloys [5,13–17], an extensive investigation was carried out by Pettit at 900–1300 °C in 0.1 atm O_2 [13]. The alloys examined were classified in three groups. The first group included alloys with low aluminum content, which formed an external NiO scale plus internal oxides of aluminum. The intermediate aluminium content alloys in the second group formed initially Al_2O_3 scales, that were later replaced by a mixture of NiO, Al_2O_3 and $NiAl_2O_4$. Finally, higher aluminium content alloys of the third group formed external Al_2O_3 scales that were retained for long periods. At 1000 °C, the minimum aluminum content required for the transition from the

first to the second group, sufficient to avoid internal oxidation of aluminum, was about 8 wt.% (15.9 at.%), while the aluminum content necessary for the transition from the second to the third group was about 17 wt.% (30.8 at.%). According to Wood and Stott [5], the critical aluminium content needed to form and retain a protective Al_2O_3 scale on binary Ni–Al alloys at 1000 °C ranges from 7 to 12.5 wt.% Al.

The oxidation of Ni–Cr alloys was also investigated extensively [3,18–22]. In particular, Giggins and Pettit [19] identified three groups of alloys. The scales formed on alloys with low chromium contents (group 1) were composed of an outermost NiO layer, followed by NiO containing some $NiCr_2O_4$ particles and a region of internal oxides of chromium. Conversely, alloys with high chromium contents (group 3) formed scales composed mainly of Cr_2O_3, while the alloy substrate was depleted in chromium. Between these two groups, there was a range of composition, extending approximately from 10 to 20 wt.% Cr (group 2), where the alloys developed irregular external scales containing mixtures of oxides of the two alloy components and the Ni–Cr spinel oxide, even though an innermost layer of Cr_2O_3 tended to form with time [19]. The oxidation rate of Ni–Cr alloys increased with increase in chromium content for dilute alloys, but decreased once the chromium content exceeded the critical value required to avoid internal oxidation of chromium. This critical chromium content was about 10 wt.% at 800–1000 °C, while that required to form exclusive external chromia scales was about 30 wt.% at 800–900 °C, but only 20 wt.% at 1000–1200 °C [19].

The oxidation of Ni–Cr–Al alloys has been studied frequently [9,23–25]. In a systematic investigation of alloys with various chromium (20–30 wt.%) and aluminum (1–9 wt.%) contents between 1000 and 1200 °C, Giggins and Pettit [9] again identified three groups of composition that followed different oxidation mechanisms. Alloys in the first group (group 1) formed an external NiO scale overlying a zone of internal oxides containing Cr_2O_3, Al_2O_3 and $Ni(Cr,Al)_2O_4$ and exhibited rapid parabolic kinetics from the beginning, with the rate constants being about an order of magnitude greater than that of pure nickel under the same conditions. Typical alloys of this group were Ni–2Cr–4Al and Ni–5Cr–1Al. Alloys in the second group (group 2) formed an external layer of Cr_2O_3 over a zone of Al_2O_3 internal oxides, while the oxidation kinetics usually obeyed a slower parabolic rate law, with rate constants close to those for growth of Cr_2O_3 scales on nickel–chromium alloys. In some cases, the instantaneous parabolic constant decreased gradually with time, to final values close to those for the growth of Al_2O_3 scales. Typical alloys of the second group were Ni–20Cr–2Al and Ni–30Cr–2Al. Finally, alloys of the third group (group 3) developed a continuous external layer of Al_2O_3 and the kinetics obeyed the parabolic rate law, with rate constants substantially smaller than those of the previous two groups but similar to those for growth of Al_2O_3scales on Ni–25Al. Typical alloys of the third group were Ni–20Cr–4Al at 1200 °C and Ni–5Cr–6Al at 1000–1200 °C. These results were summarized for each temperature on an oxide map, which superimposed on the phase diagram for the Ni–Cr–Al system three different regions (I, II and III), corresponding to the oxidation behavior of alloys in groups 1, 2 and 3, respectively [9].

Before examining the oxidation behavior predicted for the present ternary alloys, it is useful to consider first the critical contents of chromium and aluminum needed for the transition from internal oxidation of chromium or aluminium to the growth of external Al_2O_3 or Cr_2O_3 scales on binary Ni–Cr and Ni–Al alloys [N_{Cr}^{0*}(Ni–Cr) and N_{Al}^{0*}(Ni–Al)]. These calculations are carried out only for 900 °C because the situation at the two temperatures is very similar.

4.2. Critical aluminium and chromium contents for the transition to their external oxidation on binary Ni-base alloys

A calculation of the critical chromium and aluminum contents needed for the transition from internal oxidation to the formation of external chromia or alumina scales on binary Ni–Cr and Ni–Al alloys, $N_{Cr}^{o*}(1, Ni–Al)$ and $N_{Al}^{o*}(1, Ni–Cr)$, can be carried out using Wagner's criterion [11] based on the attainment of a critical value for the volume fraction of internal oxide. For binary alloys containing a reactive metal B that forms an oxide BO_v and a more noble metal A, this condition yields the equation [26]

$$N_B^{o*}(1) = f_v^* \frac{F(h_B)}{\rho(BO_v)}, \tag{1}$$

where $\rho(BO_v)$ is the ratio of the molar volumes of the alloy and the oxide BO_v (per unit mole of metal), f_v^* is the critical value for the volume fraction of internal oxide, usually set equal to 0.3 [26,27] and $F(r)$ is an auxiliary function defined as [28]

$$F(r) = \pi^{1/2} r \exp(r^2)\mathrm{erfc}(r),$$

while h_B is equal to $\gamma\varphi_B^{1/2}$, with $\varphi_B = D_O/D_B$ where D_O and D_B are the diffusion coefficients for oxygen and B in A. In turn, γ is a parameter related to the kinetics of internal oxidation through the equation [3,26]

$$\xi^2 = 4\gamma^2 D_O t, \tag{2}$$

where ξ is the distance of the internal oxidation front from the original location of the alloy surface and t is time. In the presence of an external scale of the oxide of the more noble component A (AO), γ is calculated by means of the equation [29,30]

$$\frac{N_O^{so}(A)}{v_{N_B^o}} = \frac{G(\gamma)}{F(h_B)} \frac{\mathrm{erf}(\gamma) - \mathrm{erf}(u_O)}{\mathrm{erf}(\gamma)}. \tag{3}$$

In Eq. (3), $N_O^{so}(A)$ is the concentration of oxygen in the matrix of pure A at the oxygen pressure for the equilibrium between A and AO, while u_O is defined as

$$u_O = 1/2[k_c(AO)/D_O]^{1/2}, \tag{4}$$

where $k_c(AO)$ is the parabolic rate constant for the growth of AO scales, expressed in terms of the thickness of metal consumed and $G(r)$ is another auxiliary function, defined as [28]

$$G(r) = \pi^{1/2} r \exp(r^2)\mathrm{erf}(r).$$

The data needed for this calculation are the solubility of oxygen in nickel, $N_O^{so}(Ni)$ given by [31]

$$N_O^{so}(Ni) = 8.3 \times 10^{-2} \exp(-55\ \mathrm{kJ/mol/RT}),$$

the diffusion coefficient for oxygen in nickel, $D_O(Ni)$ given by [31]

$$D_O(Ni) = 4.9 \times 10^{-2} \exp(-164\ \mathrm{kJ/mol/RT})\mathrm{cm^2 s^{-1}}$$

the diffusion coefficient for aluminium in nickel is given by [32]

$$D_{Al}(Ni–Al) = 1.0 \exp(-260\ \mathrm{kJ/mol/RT})\mathrm{cm^2 s^{-1}}$$

and the diffusion coefficient for chromium in Ni–20Cr alloys, $D_{Cr}(Ni)$, given by [33]

$$D_{Cr}(Ni) = 2.95 \times 10^{-3} \exp(-193\ \text{kJ/mol/RT}) \text{cm}^2\text{s}^{-1}$$

Another required parameter is the parabolic rate constant for growth of NiO at 900 °C. The rate constant, expressed in terms of weight-gain per unit surface area, $k_p(NiO)$, is about $9.3 \times 10^{-12}\ \text{g}^2\ \text{cm}^{-4}\ \text{s}^{-1}$ [13], which becomes equal to $1.6 \times 10^{-12}\ \text{cm}^2\ \text{s}^{-1}$ when expressed in terms of the thickness of metal consumed, $k_c(NiO)$. Finally, the molar volume of the alloy is set equal to that for pure nickel (6.59 cm^3/mol), while those for Al_2O_3 and Cr_2O_3 have been set equal to 12.86 and 14.59 cm^3 per mole of metal, respectively.

Introducing the previous data into Eqs. (1) and (3) yields $N_{Al}^{o*}(1, \text{Ni–Al}) = 11.63$ at.% and $N_{Cr}^{o*}(1, \text{Ni–Cr}) = 8.32$ at.%. The critical aluminum content calculated in this way for binary Ni–Al alloys is significantly smaller than the experimental value reported above (15.9 at.%), while the corresponding critical chromium content is close to the experimental value (10 at.%). The discrepancy between the experimental and calculated values for $N_{Al}^{o*}(\text{Ni–Al})$ probably depends on the fact that the internal alumina precipitates in Ni–Al alloys have the shape of long rods perpendicular to the alloy surface rather than forming the usual isolated round particles, making the transition to growth of alumina scales more difficult [34].

4.3. Oxidation of ternary Ni–Cr–Al alloys

The exclusive growth of external alumina scales in the oxidation of ternary Ni–Cr–Al alloys requires the avoidance of two different kinds of internal oxidation: (1) the coupled internal oxidation of aluminum and chromium beneath external NiO scales and (2) the internal oxidation of aluminum beneath external chromia scales. The corresponding critical aluminum contents are calculated separately below.

4.3.1. The transition between the coupled internal oxidation of chromium plus aluminium and their external oxidation in ternary Ni–Cr–Al alloys (Transition 1)

The calculation of the critical aluminum and chromium contents needed to prevent their coupled internal oxidation beneath external NiO scales, $N_{Cr}^{o*}(t)$ and $N_{Al}^{o*}(t)$, may be carried out using a recent extension to ternary alloys [12] of the criterion defined by Wagner [11] for the transition from internal to external oxidation of the more reactive component in binary alloys. The basis for this treatment is that the critical volume fraction needed for this transition in ternary alloys in the presence of simultaneous internal oxidation of both reactive components is given by the sum of the contributions from the two components [11,26].

For the general case of double internal oxidation of ternary A–B–C alloys where A, B and C form the oxides AO, BO_ν and CO_μ, respectively, there is the possibility of existence of either one or of two different fronts of internal oxidation [35]. In the latter case, the oxide of intermediate stability, BO_ν, precipitates at the most external front, while the most stable oxide, CO_μ, precipitates at the most internal front. For simplicity, the first hypothesis is adopted here, while possible modifications to the results due to the existence of two fronts are considered shortly below. The calculation of the critical B and C contents for the case of a single front requires the solution of a system of two equations. One of them, concerning the kinetics of this process, has the form [12,35].

$$N_O^{so} = G(\gamma)\left[\nu\frac{N_B^o}{F(h_B)} + \mu\frac{N_C^o}{F(h_C)}\right]\frac{\mathrm{erf}(\gamma) - \mathrm{erf}(u_o)}{\mathrm{erf}(\gamma)}, \quad (5)$$

where $h_C = \gamma\varphi_C^{1/2}$ with $\varphi_C = D_O/D_C$ and D_C is the diffusion coefficient of C in the alloy, while u_O is still given by Eq. (4).

The second equation needed to calculate the relation between the critical contents of B and C needed for this transition in ternary alloys, $N_B^{o*}(t)$ and $N_C^{o*}(t)$, has the form [12]

$$f_v^*(ov) = \frac{N_B^{o*}(t)\rho(BO_\nu)}{F(h_B)} + \frac{N_C^{o*}(t)\rho(CO_\mu)}{F(h_C)} \quad (6)$$

where $f_v^*(ov)$ is the critical overall volume fraction of the two internal oxides required for the transition, still set equal to 0.3, while $\rho(CO_\mu)$ is the ratio between the molar volumes of the alloy and CO_μ.

The system of Eqs. (5) and (6) can be solved for one of the two critical concentrations [e.g. $N_C^{o*}(t)$] using the bulk concentration of the other reactive component (in this case $N_B^{o*}(t)$) as an independent variable, which is allowed to change between zero and the critical value typical for binary A–B alloys. In this approximate treatment, ternary diffusion interactions are neglected for simplicity, so that the parameters involved for the ternary alloys have the same values as in the corresponding binary systems. This procedure, using the values of the parameters reported above, yields an almost linear relation between the critical contents of aluminum and chromium needed for this transition, $N_{Al}^{o*}(t)$ and $N_{Cr}^{o*}(t)$, as shown by curve a in Fig. 7. Thus, an increase in the chromium content of ternary Ni–Cr–Al alloys produces a linear decrease in the corresponding critical aluminum content. The dashed line connects the critical Al and Cr contents measured experimentally for the same transition, as reported above.

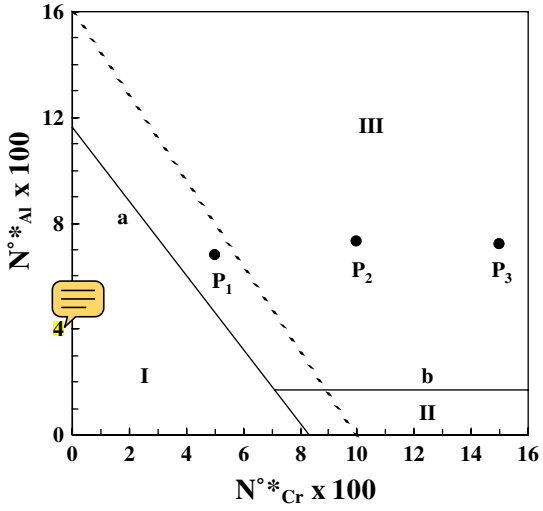

Fig. 7. Critical contents of Cr and Al needed for transition 1 beneath external NiO scales (curve a) and the critical Al content needed for transition 2 beneath external Cr_2O_3 scales (curve b) for the Ni–Cr–Al system at 900 °C. Points P_1, P_2 and P_3 correspond to the compositions of the ternary alloys examined. The dashed line connects the critical aluminium and chromium contents measured experimentally for transition 1.

In the case of precipitation of the two internal oxides at two different fronts, the parabolic rate constant related to the first front, closer to the alloy/scale interface, $k_\xi(1,II)$, becomes smaller than that calculated under the same conditions for a single front, $k_\xi(I)$, while at the same time the rate constant for the second front, deeper into the alloy, $k_\xi(2,II)$, increases with respect to $k_\xi(I)$ [35]. As a consequence of this, the degree of enrichment of B within the internal oxidation zone, $\alpha_B(II)$, increases, but only slightly, with respect to the single-front value, $\alpha_B(I)$. On the contrary, the corresponding value for C, $\alpha_C(II)$, decreases quite significantly with respect to the single-front value, $\alpha_C(I)$, due to the faster advancement of the front in the case. The net effect is that in this case transition 1 requires larger critical C contents with respect to the single-front solution for small values of N_B^o, while it tends to the same result as for the single-front solution for large N_B^o values [35]. Thus, in the presence of a double front curve a is modified as compared to the single-front solution. However, the magnitude of these effects depend on the actual value of the ratio between $k_\xi(2,II)$ and $k_\xi(1,II)$, which cannot be predicted by the present treatment [12,35]. In view of this limitation, this aspect is disregarded here, also because it would not have an important effect on the present semi-quantitative conclusions concerning the nature of the oxidation map for these alloys, presented later.

4.3.2. The transition between the internal oxidation of aluminium beneath external Cr_2O_3 scales and the growth of external alumina scales (Transition 2)

The conditions for the transition 1 considered above are not sufficient to ensure the formation of external alumina scales. In fact, in agreement with the experimental results, the addition of sufficient levels of chromium to Ni–Al alloys with a low aluminum content does not result in the growth of external alumina scales, but rather in the internal oxidation of aluminum beneath external chromia scales, so that, according to the definition by Giggins and Pettit [9], it produces a transition from region I to region II on the oxide map (transition 2). Thus, the aluminum level needed for the formation of external alumina scales must also exceed a minimum value needed for this transition, $N_{Al}^{o*}(Cr_2O_3)$, which can again be predicted by calculating the borderline between region II and region III.

According to a procedure described in a recent analysis of this problem, one of the equations needed to calculate $N_{Al}^{o*}(Cr_2O_3)$ is [36]

$$N_{Al}^{o*}(Cr_2O_3) = f_v^* \frac{F(h_{Al})}{\rho(AlO_{1.5})}, \tag{7}$$

where h_{Al} is equal to $\Gamma\varphi_{Al}$, with $\varphi_{Al} = D_O/D_{Al}$ and Γ is the kinetic parameter for internal oxidation defined by Eq. (2) as applied to the present case. Another equation involved, concerning the kinetics of internal oxidation, is [36]

$$\frac{N_O^s}{\mu N_{Al}^o} = \frac{G(\Gamma)}{F(h_{Al})} \frac{\mathrm{erf}(\Gamma) - \mathrm{erf}(U_O)}{erf(\Gamma)} \tag{8}$$

where U_O is given by

$$U_O = \frac{1}{2}\sqrt{\frac{k_c(Cr_2O_3)}{D_O}}. \tag{9}$$

An important factor in this calculation is the concentration of oxygen dissolved in the Ni–Cr matrix at the alloy/Cr_2O_3 scale interface, N_O^s. In the present case, N_O^s generally differs from the value for the Ni/NiO equilibrium, N_O^{so}, reported above, because it corresponds to the oxygen pressure for the alloy/Cr_2O_3 equilibrium and, thus, depends on the activity of chromium at the alloy/scale interface. In particular, N_O^s can be calculated from the known value of N_O^{so} using Sieverts's law [37] in the form

$$N_O^s = N_O^{so}\sqrt{\frac{P(O_2)^i}{P(O_2)(Ni/NiO)}}, \tag{10}$$

where $P(O_2)^i$ is the oxygen pressure for the alloy/Cr_2O_3 equilibrium and $P(O_2)(Ni/NiO)$ is the corresponding value for the Ni/NiO equilibrium. More precisely, $P(O_2)^i$ is a function of the chromium content in the alloy at the interface with the external Cr_2O_3 scale, N_{Cr}^i, assumed for simplicity to represent also the activity of chromium, which, in turn, depends on the bulk chromium content of the alloy, N_{Cr}^o, as well as on the rate constant for the growth of chromia scales on the alloy through the equation [30,38]

$$N_{Cr}^i = \frac{N_{Cr}^o - F(U)}{1 - F(U)}, \tag{11}$$

where

$$U = \frac{1}{2}\sqrt{\frac{k_c(Cr_2O_3)}{D_{Cr}}}. \tag{12}$$

A final equation concerns the relation between the rate constant for the growth of chromia scales and the chromium content at the alloy-scale interface: this dependence is neglected here for simplicity and, also, because it is not well known, so that $k_c(Cr_2O_3)$ is simply taken as a constant at a given temperature. In particular, according to the results of Giggins and Pettit on the oxidation of binary Ni–Cr alloys [19], the k_p value for the growth of chromia scales on Ni–20Cr at 900 °C is 1.7×10^{-12} g^2 cm^{-4} s^{-1}, which, after conversion into the corresponding value in terms of thickness of metal consumed, becomes 1.3×10^{-13} cm^2 s^{-1}. Finally, the possible effect of the presence of chromium in the Ni–Cr matrix of the internal oxidation zone on the solubility of oxygen in the alloy [39] is also neglected.

Solution of Eqs. (7), (8) and (11) with the help of Eqs. (9), (10) and (12), using the above values for the various parameters yields $N_{Al}^{o*}(Cr_2O_3)$ as a function of N_{Cr}^o, shown as curve b in Fig. 7. In the range of composition considered, $N_{Al}^{o*}(Cr_2O_3)$ is practically constant and equal to about 1.7 at.% Al. In Fig. 7, curve b is actually interrupted at its intersection with curve a, corresponding to $N_{Cr}^{o*} \cong 7.1$ at.%, because in region I curve b is virtual only.

The value of $N_{Al}^{o*}(Cr_2O_3)$ calculated above (1.7 at.%) is much smaller than that calculated above for binary Ni–Al alloys (11.63 at.%): this is a consequence of both the low values of N_O^s prevailing under external Cr_2O_3 scales compared to N_O^{so} and the lower value of $k_c(Cr_2O_3)$ compared to $k_c(NiO)$. In fact, if $N_{Al}^{o*}(Cr_2O_3)$ is calculated using the correct value of $k_c(Cr_2O_3)$, but setting $N_O^s = N_O^{so}$, $N_{Al}^{o*}(Cr_2O_3)$ around the point of intersection with curve a is about 8.3 at.%. Conversely, if $N_{Al}^{o*}(Cr_2O_3)$ is calculated using the correct value of N_O^s beneath Cr_2O_3 scales, but setting $k_c(Cr_2O_3) = k_c(NiO)$, it is about 5.1 at.%. In any case, according to the previous calculation, to produce external Al_2O_3 scales on ternary Ni–Cr–Al alloys at 900 °C, the mole fraction of aluminum must exceed about 1.7 at.%.

4.4. Final considerations

The combination of curves a and b divides the plot in Fig. 7 into three fields, which represent the regions for the coupled internal oxidation of aluminum + chromium beneath external NiO scales (region I, to the left of curve a), for the internal oxidation of aluminum beneath external Cr_2O_3 scales (region II, to the right of curve a and below curve b) and, finally, for growth of external Al_2O_3 scales (region III, to the right of curve a and above curve b). All three ternary alloys examined, represented by points P_1, P_2 and P_3 in Fig. 7, have aluminum contents above that of curve b. Moreover, all of them lie to the right of curve a and, thus, fall in the region of formation of external alumina scales, even though the alloy with 5 at.% Cr is close to curve a. However, if the ending points of curve a on the Ni–Al and Ni–Cr sides are displaced at the experimental values of $N_{Al}^{o} \cong 15.9$ at.% [13] and $N_{Cr}^{o} \cong 10$ at.% [19], the alloy with 5 at.% Cr falls to the left of curve a, corresponding to a coupled internal oxidation of Cr + Al, as observed experimentally. Thus, the oxidation behavior of the present alloys is in an acceptable qualitative agreement with the present model for the transition from internal to external oxidation of chromium and aluminum, based on an extension of Wagner's criterion to ternary alloys.

In relation to the classification of the ternary Ni–Cr–Al alloys reported by Giggins and Pettit [9], the oxidation behavior of Ni–5Cr–7Al corresponds to group 1, while Ni–10Cr–7Al corresponds to group 3. Finally, Ni–15Cr–7Al corresponds to group 3 at 900 °C, but to group 2 at 1000 °C. These results are in substantial agreement with their oxide map at 1000 °C [9], even if Ni–5Cr–7Al is very close to the boundary between group 1 and group 3. Moreover, Ni–15Cr–7Al at 1000 °C is inside group 3, but very close to the boundary with group 2, a situation in which the alloy can show a mixed type of behavior [9]. An apparently contradictory result concerns the difference in the behavior of Ni–10Cr–7Al and Ni–15Cr–7Al at 1000 °C, since the alloy with the lower chromium content forms a continuous Al_2O_3 layer beneath an outermost chromium-rich layer, while that with the higher chromium content undergoes an unusual kind of internal oxidation of aluminum, even if there is a definite tendency to form a discontinuous alumina layer. Thus, an increase in the chromium content in this range for a constant aluminum content of 7 at.% apparently favors internal rather than external oxidation of aluminum. This result is probably related to the anomalous oxidation behavior of Ni–15Cr–7Al, especially because the scale has a very variable thickness and contains large amounts of nickel, while the alloy/scale interface is very convoluted. This is apparently a case of instability of a planar alloy/scale interface, which tends to produce deep undulations of this interface, as first analyzed by Wagner [40] and later by Whittle et al. [41]. Even so, the oxidation rate of this alloy is lower than that of Ni-10Cr–7Al, indicating that the presence of Al_2O_3 in the inner region is able to affect significantly the oxidation kinetics.

The parabolic rate constants for the oxidation of Ni–5Cr–7Al are larger than those for oxidation of the binary Ni–Al alloy at both temperatures, probably mainly as a consequence of dissolution of chromium, in addition to that of aluminum, in the NiO scale, producing an increase in the concentration of cation vacancies and, thus, also in the rate constant, as already observed for both binary Ni–Al [13] and Ni–Cr [19] alloys as well as for ternary Ni–Cr–Al alloys [9]. A further contribution may also come from internal oxidation of chromium plus aluminum, rather than that of aluminum only. Conversely, the oxidation rates for the two alloys with larger chromium contents are both slower than that for Ni–7Al, and decrease, even though slightly, with the chromium content of the alloy. The

parabolic rate constants for the growth of Cr_2O_3 scales on Ni–Cr alloys change with increasing chromium content from 1.7×10^{-12} to 5.4×10^{-12} $g^2\,cm^{-4}\,s^{-1}$ at 900 °C, but are about 4×10^{-12} $g^2\,cm^{-4}\,s^{-1}$ at 1000 °C [19], while the constants for the growth of Al_2O_3 scales on Al-rich Ni–Al alloys are about 1×10^{-14} $g^2\,cm^{-4}\,s^{-1}$ at 900 °C and 7.2×10^{-14} $g^2\,cm^{-4}\,s^{-1}$ at 1000 °C [13]. Thus, the rate constants for the oxidation of Ni–10Cr–7Al and Ni–15Cr–10Al (second stages when appropriate) are intermediate between those for the growth of Cr_2O_3 and Al_2O_3 scales on the binary alloys at both temperatures. This is mainly a consequence of the formation of a layer of Al_2O_3 at the base of the scale for these alloys, even if, for Ni–15Cr–7Al at 1000 °C, this layer is apparently discontinuous.

5. Conclusions

A binary Ni–Al alloy containing about 7 at.% Al and a ternary Ni–Cr–Al alloy with the same aluminum content and 5 at.% Cr exposed to 1 atm O_2 at 900–1000 °C formed external NiO scales over zones of internal oxides of aluminium and aluminium plus chromium, respectively. Conversely, ternary alloys containing 7 at.% Al with 10 and 15 at.% Cr formed external scales composed of an outer layer rich in chromium and an inner layer rich in aluminum, while internal oxidation was suppressed. Thus, a chromium addition ranging between 5 and 10 at.% to Ni–7Al is sufficient to prevent the internal oxidation of aluminum and to induce the formation of external Al_2O_3 scales, providing an example of the third-element effect. Calculation of the critical aluminum content needed to avoid its internal oxidation and to form external Al_2O_3 scales on ternary Ni-Cr–Al alloys, using an extension to ternary alloys of the criterion proposed by Wagner for the same transition in binary alloys, based on the attainment of a critical value for the overall volume fraction of internal oxides of chromium and aluminum, is in substantial agreement with the oxidation behavior observed for these alloys.

Acknowledgements

Financial supports by the National Natural Scientific Foundation of China (NSFC) under the grants (Nos. 50271079 and 50571107) are gratefully acknowledged.

References

[1] F.H. Stott, G.C. Wood, J. Stringer, Oxid. Met. 44 (1995) 113.
[2] F.H. Stott, Rep. Progr. Phys. 50 (1987) 861.
[3] P. Kofstad, High Temperature Corrosion, Elsevier Science, New York, 1987.
[4] W.E. Boggs, J. Electrochem. Soc. 118 (1971) 906.
[5] G.C. Wood, F.H. Stott, Br. Corros. J. 6 (1971) 247.
[6] G.N. Irving, J. Stringer, D.P. Whittle, Oxid. Met. 9 (1975) 427.
[7] H. Hindam, D.P. Whittle, Oxid. Met. 18 (1982) 245.
[8] E.W. Ross, C.T. Sims, in: C.T. Sims, N.S. Stoloff, W.G. Hagel (Eds.), Superalloys II, Wiley Interscience, New York, 1987 (Chapter IV).
[9] C.S. Giggins, F.S. Pettit, J. Electrochem. Soc. 118 (1971) 1782.
[10] C. Wagner, Corros. Sci. 5 (1965) 751.
[11] C. Wagner, Z. Elektrochem. 63 (1959) 772.
[12] Y. Niu, F. Gesmundo, Oxid. Met. accepted for publication.
[13] F.S. Pettit, Trans. Metall. Soc. AIME 239 (1967) 1296.
[14] J.D. Kuenzly, D.L. Douglass, Oxid. Met. 8 (1974) 139.

[15] J.L. Smialek, Met. Trans. 9A (1978) 309.
[16] H.M. Hindam, W.W. Smeltzer, J. Electrochem. Soc. 127 (1980) 1622.
[17] W.W. Smeltzer, H.M. Hindam, F.A. Elrefaie, in: R.A. Rapp (Ed.), High Temperature Corrosion, NACE, 1983, pp. 251.
[18] N. Birk, H. Richert, J. Inst. Met. 91 (1962–1963) 308.
[19] C.S. Giggins, F.S. Pettit, Trans. Met. Soc. AIME 245 (1969) 2495.
[20] G.R. Wallwork, A.Z. Hed, Oxid. Met. 3 (1971) 171.
[21] G.M. Ecer, G.H. Meier, Oxid. Met. 13 (1979) 119.
[22] S. Espevik, R.A. Rapp, P.L. Daniel, J.P. Hirth, Oxid. Met. 14 (1980) 85.
[23] F.H. Stott, G.C. Wood, Corros. Sci. 11 (1971) 799.
[24] F.H. Stott, G.C. Wood, M.G. Hobby, Oxid. Met. 3 (1971) 103.
[25] I.A. Kvernes, P. Kofstad, Met. Trans. 3 (1972) 1511.
[26] R.A. Rapp, Corrosion 21 (1965) 382.
[27] R.A. Rapp, Acta Met. 10 (1961) 730.
[28] J. Crank, The Mathematics of Diffusion, Oxford University Press, New York, 1994.
[29] F. Gesmundo, F. Viani, Oxid. Met. 25 (1986) 269.
[30] F. Gesmundo, Y. Niu, Oxid. Met. 50 (1998) 1.
[31] J.W. Park, C.J. Altstetter, Met. Trans. 18A (1987) 43.
[32] W. Gust, M.B. Hintz, A. Lodding, H. Odelius, B. Predel, Phys. Stat. Sol. 64 (1981) 187.
[33] M.S. Seltzer, B.A. Wilcox, Met. Trans. 3 (1972) 2357.
[34] A. Martinez-Villafane, F.H. Stott, J.C. Chacon-Nava, G.C. Wood, Oxid. Met. 57 (2002) 267.
[35] Y. Niu, F. Gesmundo, Oxid. Met. 62 (2004) 341.
[36] Y. Niu, F. Gesmundo, Oxid. Met. 62 (2004) 391.
[37] D.R. Gaskell, Introduction to Thermodynamics of Materials, Taylor and Francis, Washington, 1995.
[38] C. Wagner, J. Electrochem. Soc. 99 (1952) 369.
[39] F. Gesmundo, Y. Niu, Oxid. Met. 60 (2003) 347.
[40] C. Wagner, J. Electrochem. Soc. 103 (1956) 571.
[41] D.P. Whittle, D.J. Young, W.W. Smeltzer, J. Electrochem. Soc. 123 (1976) 1073.